Structure of an HIV-1–neutralizing antibody target, the lipid-bound gp41 envelope membrane proximal region trimer

Patrick N. Reardon[a,1], Harvey Sage[a], S. Moses Dennison[b], Jeffrey W. Martin[c], Bruce R. Donald[a,c], S. Munir Alam[b], Barton F. Haynes[b], and Leonard D. Spicer[a,d,2]

[a]Department of Biochemistry, [b]Duke Human Vaccine Institute, Duke Department of Medicine, and [d]Department of Radiology, Duke University School of Medicine, Durham, NC 27710; and [c]Department of Computer Science, Duke University, Durham, NC 27708

Edited* by William F. DeGrado, University of California, San Francisco School of Pharmacy, San Francisco, CA, and approved December 5, 2013 (received for review June 7, 2013)

The membrane proximal external region (MPER) of HIV-1 glycoprotein (gp) 41 is involved in viral–host cell membrane fusion. It contains short amino acid sequences that are binding sites for the HIV-1 broadly neutralizing antibodies 2F5, 4E10, and 10E8, making these binding sites important targets for HIV-1 vaccine development. We report a high-resolution structure of a designed MPER trimer assembled on a detergent micelle. The NMR solution structure of this trimeric domain, designated gp41-M-MAT, shows that the three MPER peptides each adopt symmetric α-helical conformations exposing the amino acid side chains of the antibody binding sites. The helices are closely associated at their N termini, bend between the 2F5 and 4E10 epitopes, and gradually separate toward the C termini, where they associate with the membrane. The mAbs 2F5 and 4E10 bind gp41-M-MAT with nanomolar affinities, consistent with the substantial exposure of their respective epitopes in the trimer structure. The traditional structure determination of gp41-M-MAT using the Xplor-NIH protocol was validated by independently determining the structure using the DISCO sparse-data protocol, which exploits geometric arrangement algorithms that guarantee to compute all structures and assignments that satisfy the data.

Infection of a $CD4^+$ T cell by HIV-1 is mediated by the envelope protein (Env), a trimeric complex located on the virion surface that consists of three copies each of glycoprotein (gp) 120 and gp41. This complex is a macromolecular machine responsible for host-cell recognition followed by fusion of the viral and $CD4^+$ T-cell membranes, leading to virus entry (1). The Env complex represents the primary target for antibody-mediated viral neutralization (2).

The Env protein complex undergoes dramatic conformational changes during the process of membrane fusion. Biochemical and structural evidence suggests that membrane fusion involves at least three states of the Env complex (3, 4). The first state is the resting prefusion state that exists before host-cell encounter and receptor binding. This state has been studied by several groups using cryo-EM (5–10). The second state is a prefusion intermediate where gp41 is interacting with both the host cell and viral membranes. This prefusion intermediate, or a closely related intermediate, is also believed to be the target for fusion-inhibiting peptides (11) as well as the broadly neutralizing antibodies 2F5 and 4E10 (12). The final state is the postfusion or six-helix bundle. The formation of this conformation is thought to drive membrane fusion. This conformation is stable, and its structure has been well studied using X-ray crystallography techniques (13). Binding studies have shown that the broadly neutralizing antibodies 2F5 and 4E10 do not bind with high affinity to either the postfusion six-helix bundle or the prefusion resting state, suggesting that a prefusion intermediate state is the target for these antibodies (12).

The membrane proximal external region (MPER) is a 28-residue segment of each subunit in the gp41 homotrimer. This tryptophan-rich segment is juxtaposed to the transmembrane domain and plays an important role in the membrane-fusion process leading to viral infection of the host cell (14, 15). The MPER contains the binding epitopes for several broadly neutralizing antibodies, including 2F5, 10E8, and 4E10 (16-18). This observation has motivated efforts to develop vaccines designed to induce antibodies specific to this region. Vaccine candidates based on linear peptides from the MPER (19), trimeric gp41 constructs (20, 21), and conformationally constrained peptides have been previously reported (22, 23). In animal models, many of these vaccine designs have elicited antibodies that recognize epitopes in the MPER (19, 22, 23). However, none of the induced plasma antibodies strongly neutralize HIV-1 (19, 20, 23, 24), either because the trial vaccines do not present the epitope residues in a native conformation or in the presence of the correct molecular environment, or because of the limitation of induction of MPER antibodies by host tolerance mechanisms (25–28).

The mAbs 2F5 and 4E10 are polyreactive for non–HIV-1 proteins and for lipids (29, 30). Crystal structures of 2F5 and 4E10 Fab domains bound to short epitope-containing MPER peptides show limited CDR-H3 contacts with the MPER peptides

Significance

A major roadblock in the development of an HIV vaccine is the need to develop vaccine regimens that will induce antibodies that bind to conserved regions of the HIV envelope and neutralize many different virus quasispecies. One such envelope target is at the region closest to the membrane, the glycoprotein (gp) 41 membrane proximal external region (MPER). Previous work has demonstrated that antibodies that target this region bind both to the gp41 polypeptide and to the adjacent viral membrane. However, what has been missing is a view of what the MPER-neutralizing epitopes may look like in the context of a trimeric orientation with lipids. We have constructed an MPER trimer associated with lipids and solved the trimer structure by NMR spectroscopy.

Author contributions: P.N.R., H.S., S.M.D., J.W.M., B.R.D., S.M.A., B.F.H., and L.D.S. designed research; P.N.R., H.S., S.M.D., and J.W.M. performed research; P.N.R., H.S., S.M.D., J.W.M., B.R.D., S.M.A., B.F.H., and L.D.S. analyzed data; and P.N.R., H.S., S.M.D., J.W.M., B.R.D., S.M.A., B.F.H., and L.D.S. wrote the paper.

The authors declare no conflict of interest.

*This Direct Submission article had a prearranged editor.

Freely available online through the PNAS open access option.

Data deposition: The atomic coordinates have been deposited in the Protein Data Bank, www.pdb.org [PDB ID codes 2LP7 (Xplor-NIH–based ensemble) and 2M7W (DISCO-based ensemble)]. The NMR chemical shifts and restraints have been deposited in the BioMagResBank, www.bmrb.wisc.edu (accession no. 18237).

[1]Present address: Environmental Molecular Sciences Laboratory, Pacific Northwest National Laboratory, Richland, WA 99354.

[2]To whom correspondence should be addressed. E-mail: spicer@biochem.duke.edu.

This article contains supporting information online at www.pnas.org/lookup/suppl/doi:10.1073/pnas.1309842111/-/DCSupplemental.

and, together with the lipid-reactive data, prompted speculation that the long hydrophobic CDR-H3 loops in the antibodies contact the viral membrane (31–33). Mutations of some of the hydrophobic residues in the CDR-H3 regions reduce the lipid-binding activity of these antibodies without reducing peptide binding, but these mutants are also nonneutralizing for HIV-1 (34–36). These data demonstrated that association with the viral membrane plays an important role in the molecular mechanism for viral neutralization by 2F5 and 4E10 (34).

Here, we report the biosynthesis and structure determination of a micelle-bound MPER trimer in a putative prefusion intermediate state. The designed trimer readily associates with dodecylphosphocoline (DPC) micelles and 1,2-dimyristoyl-*sn*-glycero-3-phosphocholine (DMPC) liposomes. The solution NMR structure reported is an atomic level representation of the MPER trimer that is complexed directly with the outer surface of the micelle. This trimer, displayed on both liposomes and micelles, avidly binds the 2F5 and 4E10 neutralizing antibodies. We also observe conformational flexibility within the polypeptide subunits that we hypothesize is important for binding to the 2F5 and 4E10 antibodies based on the crystal structures of the antibodies bound to short peptide epitopes.

Results

Trimer MPER Construct and NMR Structure. We designed the gp41 MPER trimer construct based on a chimeric polypeptide monomer containing the 27-residue trimerization domain from bacteriophage T4 fibritin (the foldon domain) N-terminal to the MPER sequence (NEQELLELDKWASLWNWFNITNWLWYIK), corresponding to residues 656–683 of Hxb2 HIV-1. The foldon domain is linked to the MPER domain via a flexible Gly-Ser-Ser-Gly linker, allowing the MPER to adopt orientations with minimal constraint from the foldon. The polypeptide spontaneously trimerizes and directly associates with the phospholipid membrane surface at the MPER C terminus, where the transmembrane segment of gp41 begins in the full-length protein. This transmembrane domain consists of 31 residues that are not included in our construct. A schematic diagram of the gp41 MPER containing Membrane Associated Trimer (designated gp41-M-MAT) is shown in Fig. 1*B*.

The solution structure of the membrane-associated gp41-M-MAT was determined using NOE-based distance restraints, dihedral angles, ^{3}J-coupling constants, and HN residual dipolar coupling data collected at 600, 800, and 950 MHz (summarized in Table S1). The ^{15}N-TROSY HSQC spectrum revealed a single set of amide moiety resonances, which facilitated the assignments and indicated that the trimer was symmetric. Based on the HN residual dipolar coupling (RDC) data, the calculated rhombicity of the trimer on the micelle was 0.052, consistent with a symmetric homotrimer, where the ideal rhombicity is zero. Further analysis of these data revealed that the separate foldon and MPER domains adopted the same symmetry axis orientations, within experimental error. Representative data from the RDC experiments and a summary of the symmetry axis analysis are shown in Fig. S1. The solution structure we determined for gp41-M-MAT is shown in Fig. 2. A comparison of the structures computed by Xplor-NIH and the alternative DISCO method is shown in Fig. 3. Importantly, these two alternative methods result in nearly identical trimeric architectures for the MPER. The most significant differences in the structural ensembles derived by the two methods are in the flexible linkers. These differences lead to increased rmsds between the two gp41-M-MAT ensembles because the conformational variations in the linkers allow increased rotational freedom around the symmetry axis that results in a small range of relative rotations for the foldon and MPER domains.

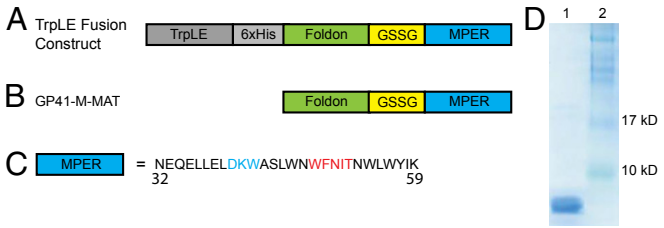

Fig. 1. gp41-M-MAT design and purification. (*A*) The gp41-M-MAT peptide is expressed as a TrpLE fusion construct in C41(DE3) *E. coli* cells. The TrpLE tag directs the polypeptide into inclusion bodies, which facilitates expression and purification. (*B*) gp41-M-MAT after cyanogen bromide cleavage to remove the TrpLE tag. (*C*) Peptide sequence of MPER used in the gp41-M-MAT. The MPER residues are numbered 32–59 in gp41-M-MAT, which corresponds to residues 656–683 of HXB2 HIV-1. Epitopes for 2F5 (D40-W42) and 4E10 (W48-T52) are shown in blue and red, respectively. (*D*) The 16.5% Tris-Tricine SDS/PAGE of purified gp41-M-MAT (lane 1). Molecular mass markers are shown in lane 2.

Each subunit of the MPER trimer is in an α-helical conformation ~40 Å long. The three helices form a threefold symmetric left-handed bundle that progressively expands from residue 32 where the Cα atoms of each helix are separated by 14 Å to a C-terminal separation of ~30 Å between Cα positions in residue 59. Intermolecular NOEs are observed between the side chains of residues 39 and 42 and the backbone amide of residue 38. Amino acid residues 39 and 42 are highly conserved in the MPER (see Fig. S7). Additional intermolecular NOEs were not observed for residues 29–37 likely due to increased dynamics in this region. The observed chemical shifts of the foldon domain in gp41-M-MAT were consistent with those reported for trimerized foldon, confirming that the foldon was folded and trimerized (37). The gp41-M-MAT on the micelle exhibits unique architecture compared with other gp41 trimer designs that incorporate nonnative C-terminal trimerization domains (12, 20, 21, 38).

The 2F5 epitope core residues D40, K41, and W42 are highlighted in Fig. 2 *B* and *C*, showing that they are accessible for antibody binding. Residues D40 and K41 are on the surface of gp41-M-MAT, with part of the W42 side chain oriented toward the axis of symmetry, leaving the rest at least partially solvent exposed. The individual members of the calculated ensembles from both 2LP7 and 2M7W exhibit varying degrees of solvent exposure for W42 due to the limited side-chain constraints observed. Interestingly, the least conserved residue in the 2F5 core epitope, K41, is oriented directly away from the trimer interface toward the bulk solvent. The structural conformation of the 2F5 epitope in gp41-M-MAT exhibits little similarity with that observed in crystal structures of short MPER peptide segments bound to 2F5 Fabs (31).

The 4E10 epitope region, W48–T52, highlighted in Fig. 2 *B* and *D*, is helical in our NMR structure. In the crystal structure of 4E10 bound to short epitope-containing peptides W48, F49, I51, and T52 are in a helical conformation and account for the most contacts between the peptide and the antibody (32). Fig. 2*D* shows that the side chain of F49 in our construct is directed inward toward the axis of symmetry, potentially contacting the micelle (see *Micelle Occupancy and Localization*). This orientation is similar to that proposed for F49 in the linear MPER peptide monomer structure, 2PV6, which suggested that F49 is buried in the lipid or micelle (39). N50 is exposed on the outer surface and is somewhat less conserved than the other residues in the epitope (32, 40). In the crystal structure, this residue makes fewer contacts with 4E10 compared with most of the other residues in the peptide epitope (32).

Binding to HIV-1–Neutralizing Antibodies. Binding of 2F5 and 4E10 intact bivalent antibodies and Fabs to the gp41-M-MAT construct displayed on DPC micelles and DMPC liposomes was assayed using equilibrium analytical ultracentrifugation (AUC) and surface plasmon resonance (SPR). AUC of the trimer/micelle

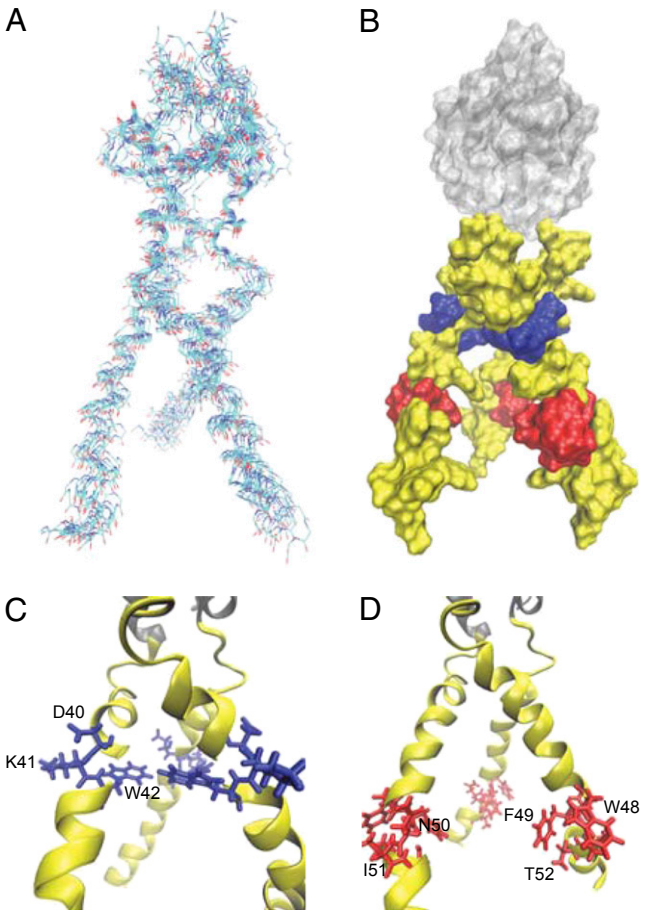

Fig. 2. NMR Structures of gp41-M-MAT (2LP7) (*A*) Overlay of 11 low-energy gp41-M-MAT structures containing no NOE violations or dihedral violations of greater than 0.5 Å or 5°, respectively. (*B*) Space-filling diagram of the minimized average structure with the 2F5 and 4E10 epitopes colored in blue and red, respectively. The exogenous trimerization domain is shown in translucent light gray. (*C* and *D*) Detailed views emphasizing the epitopes for 2F5 in blue (*C*) and 4E10 in red (*D*).

complex with 2F5 Fabs gives a buoyant molecular mass of 33,341 Da, which corresponds well with the expected buoyant molecular mass for a 3:1 complex of 36,357 Da, indicating that gp41-M-MAT binds up to three 2F5 Fabs (Fig. 4 and Table S2). At Fab:gp41-M-MAT ratios greater than 3:1, the buoyant molecular weight decreases due to saturation of the available binding sites and the subsequent observation of additional free antibody. AUC data collected at various ratios of 2F5 Fab to gp41-M-MAT in DPC micelles fit an association model with three independent binding sites on gp41-M-MAT, each having a binding constant of ~143 nM for 2F5 Fab binding to gp41-M-MAT. Representative AUC data and the corresponding fit generated by the model are shown in Fig. S2.

The SPR sensograms of monoclonal 2F5 and 4E10 full antibodies binding to gp41-M-MAT-liposome conjugates over a range of antibody concentrations are shown in Fig. 5. These data give apparent binding constants of 0.18 nM and 27 nM, respectively, for 2F5 and 4E10 (Table S2). Clear SPR profiles were observed for 2F5 and 4E10 binding to the trimer on DPC micelles although quantitation was compromised by the excessive drift in the signal due to detergent in the fluid phase. Based on the AUC result above, 2F5 Fab binding to the MPER trimer/micelle conjugate appears to be weaker than binding of the full antibody to the corresponding liposome conjugate.

A new broadly neutralizing antibody, 10E8, that binds the C-terminal segment of the MPER has recently been reported (18). Its recognition site includes residues within the 4E10 epitope, but it does not bind phospholipids and may have the potential to escape immune tolerance associated with membrane binding. Although its affinity for the MPER is lower than 2F5 or 4E10, its neutralization capacity is similar to 4E10; however, unlike 4E10, it binds cell-surface envelope spikes (18). These observations suggest that 10E8 targets the initial prefusion conformational state of gp41 rather than the prefusion intermediate state that gp41-M-MAT was designed to potentially represent. SPR binding curves shown in Fig. S3 indicate that 10E8 interacts poorly with gp41-M-MAT. In the structure of gp41-M-MAT, the side chains of residues F49, W56, and K59 are oriented toward the micelle, which may contribute to the lack of 10E8 binding to gp41-M-MAT (Fig. S4). In contrast, lipid binding by 2F5 and 4E10 may allow these antibodies to interact with amino acid residues that are also in contact with the micelle, resulting in high-affinity binding. This binding data further supports the hypothesis that 4E10 and 10E8 antibodies neutralize virus by binding distinctly different conformations of the gp41 MPER, suggesting that each antibody may be useful in probing molecular models for vaccine design.

Micelle Occupancy and Localization. The detergent soluble paramagnetic probe 16-DOXYL-stearic acid (DSA) was used to reveal the regions of gp41-M-MAT that interact with the DPC detergent micelle (41–43). DSA is a paramagnetic probe that localizes to the hydrophobic interior of detergent micelles and membranes where it enhances relaxation of resonances from residues that are in proximity to the micelle or membrane. Resonances that are relaxed by DSA are identified by the reduction of the intensity of the resonance in the presence of DSA vs. in the absence of DSA. DSA will relax resonances of polypeptide residues on the surface or interior of the micelle at concentrations of one or two molecules per micelle (41). NMR signals from residues 36 through 59 in the micelle-bound trimer

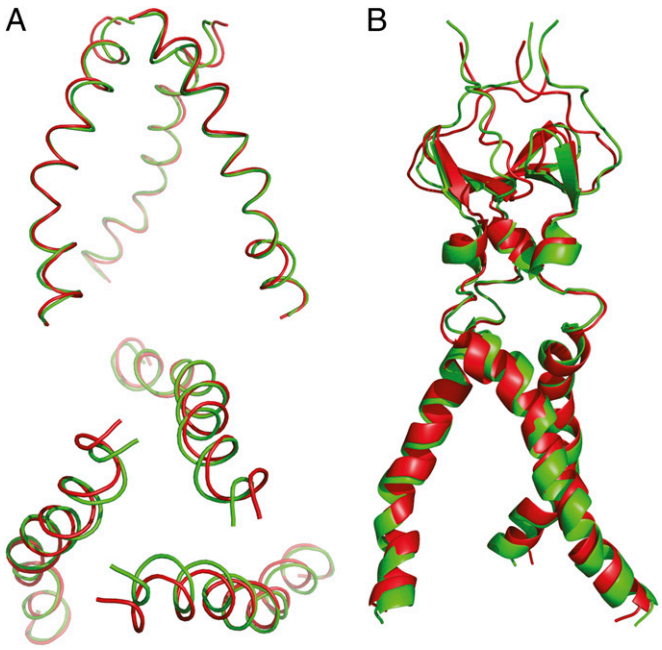

Fig. 3. Comparison of gp41-M-MAT structures calculated with Xplor-NIH (2LP7) and DISCO (2M7W). Best pairwise backbone alignments of the ensembles computed by Xplor-NIH (red) and DISCO (green) for (*A*) the MPER and (*B*) the full-length gp41-M-MAT. The rmsds for *A* and *B* are 1.07 Å and 1.66 Å, respectively.

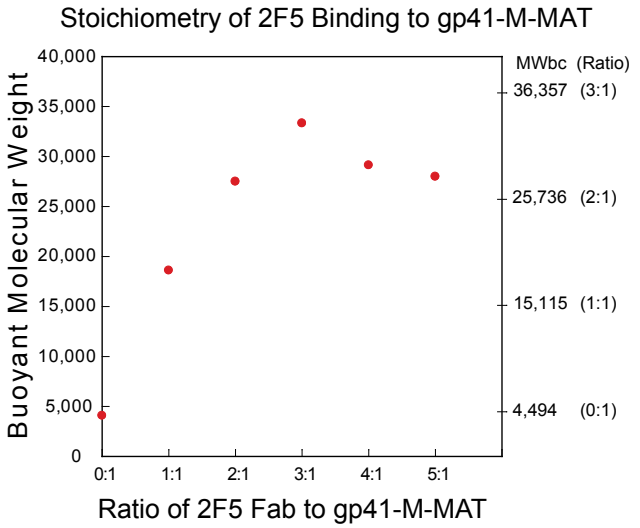

Fig. 4. Analytical ultracentrifugation results. Determination of the stoichiometry of 2F5 Fab binding to gp41-M-MAT trimer. The buoyant molecular weights of various ratios of 2F5 Fab and gp41-M-MAT were determined in 50 mM sodium phosphate, 5 mM DPC, and 58% D_2O using equilibrium analytical ultracentrifugation. Note the curve peaks at a ratio of 3:1 Fab:trimer The data shown were collected at 8,000 rpm and fit to an ideal species model to obtain the buoyant molecular weights. Expected buoyant molecular weights (MWbc) for various ratios of Fab to gp41-M-MAT (shown in parentheses) are indicated on the right hand axis.

are significantly relaxed by DSA although residues 1 through 27 are relatively unperturbed, as illustrated in Fig. 6. There are no significant chemical-shift perturbations observed in the spectrum with DSA, providing evidence that the DSA is not binding directly to the hydrophobic MPER region of gp41-M-MAT. These data indicate that the C-terminal region of the MPER peptide in gp41-M-MAT is associating with the detergent micelle, suggesting that the micelle resides in or near the cavity formed by the splayed MPER helices, with the side chains of residues W56, F49, and W46 in position to interact with the micelle. A schematic model for the positioning of gp41-M-MAT on the surface of micelles is shown in Fig. S4. We measured the mass of detergent bound to gp41-M-MAT using analytical ultracentrifugation at various solvent densities as described in *Materials and Methods*. This analysis revealed that gp41-M-MAT binds one DPC micelle per trimer (Fig. S2).

Dynamics of the MPER Trimer. Heteronuclear HN NOE data were used to probe the flexibility of gp41-M-MAT. Fig. 7 summarizes the results of these experiments. These data indicate that the MPER domain exhibits significant dynamic behavior patterns whereas the foldon is relatively rigid. From the N terminus to the 2F5 epitope (residues 32–39), the data are consistent with fast internal motion. The core 2F5 epitope region (residues 40–42) is less dynamic whereas the region between the 2F5 epitope and the 4E10 epitope (residues 43–47) is relatively rigid. Backbone mobility increases slightly at residue 48 in the 4E10 epitope (residues 48–52).

An important design feature of gp41-M-MAT included a flexible linker at residues 28–31, between the foldon trimerization domain and the MPER, that is intended to minimize the effect of the structured foldon on the conformation and dynamics of the MPER trimer subunits. It is clear from the heteronuclear NOE data that the linker exhibits increased flexibility compared with the foldon domain. Taken together with the absence of secondary structure observed for the linker, these data indicate that the foldon helix does not nucleate helix formation in the MPER.

Discussion

General physical properties and antibody-binding characteristics of several gp41 MPER-derived peptides have been reported, including at least three trimeric constructs in an extended conformation hypothesized to be similar to the prefusion intermediate state (12, 20, 21), the putative target of 2F5 and 4E10 antibodies (12). Two of these trimeric constructs are reported to induce antibodies that react with the MPER when administered to rodents (20, 21); however, these antibodies are nonneutralizing.

Structural studies of the MPER domain have been limited primarily to short, monomeric peptide sequences and two trimeric constructs. The short peptides were either solubilized in detergent micelles (39, 44, 45) or in bound forms cocrystallized with MPER-recognizing antibodies (31, 32). Of the trimeric structures, one was not membrane-associated and does not bind 2F5 or 4E10 antibodies (38), and the other was part of a six-helix bundle representing the postfusion state of gp41 (13).

The gp41-M-MAT construct characterized here does not incorporate the C-terminal transmembrane domain of gp41, but it does associate directly with micelles and liposomes. We note that, in the virus, the trimerization state of the transmembrane domain that immediately follows the MPER domain is not well-characterized. Some cryo-EM studies of intact Env show evidence for little or no trimerization of the the transmembrane domain (5, 8). Others are consistent with a more compact structure having a width of ~35 Å where the Env stalk enters the membrane (6, 7, 10). The crystal structure of the postfusion six-helix bundle shows that the MPER packs onto the outside of the bundle, leading to significant separation of the C termini of the MPER domain (13). In our structure, the C termini of the MPER trimer segments are not self-associated and, instead, are associated with the detergent micelle. Our structure may represent an intermediate state where the transmembrane domain is not tightly bundled, allowing the MPER to associate with the viral membrane in conformations that enable its important function in the membrane-fusion process (14, 15). Thus, it will be of interest to determine the status of the MPER in atomic level structures of intact gp41-gp120 trimers.

Structure determination of multimeric membrane-associated proteins in solution is challenging, and very few structures have been reported. In general the large size of the assembly and the unfavorable spin relaxation of systems like micelle solubilized proteins often limit the structural restraints observed in NMR. To determine the gp41-M-MAT structure, we combined traditional NMR structure determination techniques with recently reported methods based on residual dipolar couplings (46).

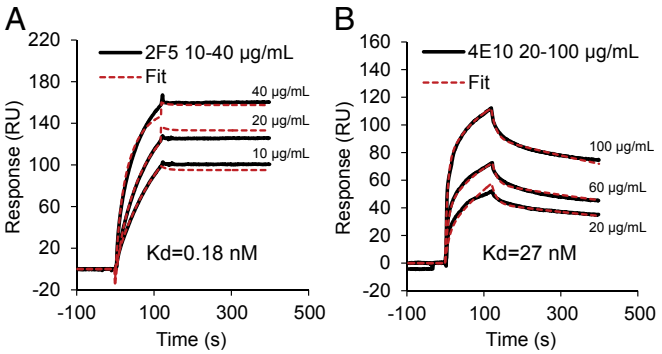

Fig. 5. SPR sensograms for titrations of antibodies with gp41-M-MAT conjugated to liposomes. The K_d values for 2F5 (*A*) and 4E10 (*B*) binding (shown in each panel) were determined by measuring binding kinetics at the indicated concentrations of antibody and globally fitting the data to a two-step encounter docking model. The titration data shown are from a representative single experiment. The K_d values were in the range of 0.9–1.2 nM for 2F5 and 17–25 nM for 4E10 mAbs, respectively, from independent experiments performed on different batches at single concentrations of antibodies.

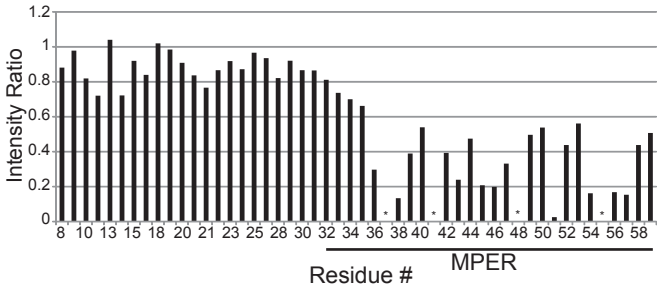

Fig. 6. Paramagnetic relaxation enhancement by 16-doxyl stearic acid (DSA). ^{15}N-TROSY HSQC spectra were collected with or without 0.5 mM DSA. For each backbone amide resonance, the ratio of peak intensities with and without DSA was determined (plotted on the vertical axis). Resonances in the MPER that could not be observed due to spectral overlap are indicated by an *. Prolines and N-terminal resonances in the foldon domain that could not be observed due to deficiencies in spectral quality were omitted.

Two intermolecular NOEs would be insufficient to pack the helices for a general multimeric structure. Indeed, without any additional constraint, the space of possible packings between two helices has six degrees of freedom: rotations and translations ($\mathbb{R}^3 \times \boldsymbol{SO}(3)$). However, in the case of a symmetric homo-trimer, such as the MPER in gp41-M-MAT, after the orientation of the symmetry axis has been determined, the constraint imposed by the symmetry reduces the dimensionality to two degrees of freedom: positions of the symmetry axis relative to the subunit structure ($\mathbb{R}^2$) (46). With two degrees of freedom instead of six, far fewer intersubunit restraints are needed to define the helical packing. For the MPER trimer, we show in Figs. S5 and S6 that two NOEs are sufficient to pack the interface.

The DISCO approach treats symmetry differently than Xplor-NIH. In Xplor-NIH, a potential that penalizes differences among the subunit structures, along with a potential encoding intersubunit distance restraints, is used to implicitly represent the symmetry axis. In contrast, DISCO explicitly models the symmetry by computing the parameters of the symmetry axis directly and thus defines a simpler structure-determination problem. Under this parameterization, every possible quaternary structure satisfies the symmetry, and all that remains is to compute the subset of symmetric quaternary structures that satisfy the experimental restraints. When the symmetry and the experimental restraints are simultaneously satisfiable, and when Xplor-NIH discovers satisfying quaternary structures without falling into a local-energy minimum, the two approaches will return similar answers (see Table S3 for comparisons). The advantage of the parametric representation is that all satisfying quaternary structures can be reported, or it can be proven that none exist.

Based on the NMR structure of gp41-M-MAT, it is apparent that the structure of the 2F5 epitope in the MPER trimer differs from the structure of the epitope observed in the cocrystal structure of 2F5 Fab bound to a short MPER-derived linear peptide (shown in Fig. S7) and the NMR structure of the linear MPER peptide in a micelle (Fig. S7). In the 2F5 cocrystal structure, the MPER fragment exhibits a β-hairpin at the core 2F5 epitope (31) whereas, in gp41-M-MAT on DPC micelles, the 2F5 epitope has an α-helical conformation. The binding affinity to 2F5 in both cases, however, is in the nanomolar range. In contrast, the helical conformation of the 4E10 epitope in gp41-M-MAT is similar to that observed in the cocrystal structure of the short peptide bound to 4E10 Fab (32). In our trimeric complex, the main residues that would contact 4E10, W48 and I51, are exposed on the surface whereas the side chains of F49 and T52 are oriented toward the micelle, like that observed for a linear MPER peptide monomer on the surface of a detergent micelle (39). The affinity of our trimeric construct for 4E10 Mab is consistent with the 4E10 affinities observed for linear MPER peptides displayed on liposomes (47).

Superposition of the gp41-M-MAT epitopes onto the respective 2F5 and 4E10 Fabs at the epitope recognition sites in the crystal structures (31, 32) produced significant steric clashes with other parts of the MPER domain. In both 2F5 and 4E10, the residues N-terminal of their respective epitopes in gp41-M-MAT clash with large portions of the antibody. The clashes observed are extreme and show that docking of the gp41-M-MAT structure onto the epitopes in the crystal structures does not produce a realistic representation of antibody binding to gp41-M-MAT, suggesting that the MPER domain in our construct undergoes significant conformational changes that turn the N-terminal region of the MPER away from the antibody upon binding. Importantly, gp41-M-MAT binds 2F5 and 4E10 with high affinity, demonstrating that the helical conformation in our NMR structure does not inhibit antibody binding. Instead, the increased dynamic flexibility observed in our structure at the 2F5 and 4E10 binding sites may allow the MPER sufficient mobility to alter its conformation upon antibody binding and turn the N-terminal region of the MPER away from the antibody to avoid steric clashes. This flexibility is important for HIV-1 vaccine development because a rigid vaccine candidate may not be able to mimic this behavior and may consequently fail to induce 2F5- or 4E10-like antibodies. Furthermore, all three 2F5 epitopes on gp41-M-MAT trimer bind 2F5 with high affinity, making gp41-M-MAT a unique multivalent antigen that effectively presents the MPER epitopes for recognition and high-affinity binding.

This unique gp41-M-MAT design and structure represent an antigenic, trimeric MPER domain directly associated with the lipid membrane without an exogenous trimerization domain at the C terminus. It provides important structural information that can further illuminate HIV vaccine development efforts. Finally, the structure of gp41-M-MAT is an important addition to the relatively small number of multimeric membrane-associated structures determined using solution-state NMR.

Materials and Methods

Gp41-M-MAT was expressed into inclusion bodies using a TrpLE tag in C41 (DE3) *Escherichia coli*. For NMR samples, cells were grown in stable isotope (^{2}H, ^{13}C, and/or ^{15}N)-labeled minimal media supplemented with 10% (vol/vol) stable isotope-labeled bioexpress rich media (Cambridge Isotopes). Gp41-M-MAT was purified under denaturing conditions in 6 M guanidine-HCl. TrpLE was removed using CNBr cleavage for 2 h in 70% (vol/vol) TFA. Samples were prepared in DPC detergent and 50 mM sodium phosphate, pH 6.0. Liposome conjugates were formed by mixing gp41-M-MAT in 6 M guanidine-HCl with preformed unilamellar vesicles and removing the denaturant via dialysis. See *SI Materials and Methods* for detailed sample preparation procedures.

Analytical ultracentrifugation data were collected at multiple rotor speeds using absorbance optics on a Beckman XL-A. Density matching was used to

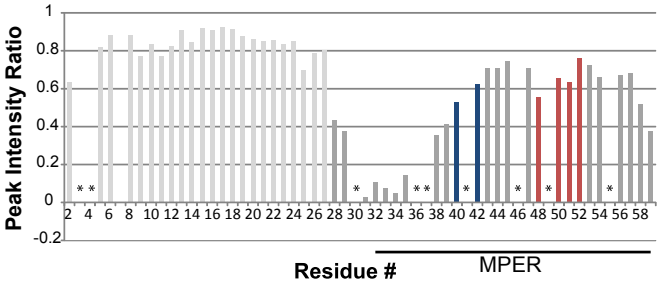

Fig. 7. Summary of HN-heteronuclear NOE data. The plot shows the ratio of the cross-peak intensities with and without proton saturation (3 s). The 2F5 and 4E10 core epitopes are shown in blue and red, respectively. The region corresponding to the foldon domain is colored light gray. *, indicates resonances that could not be clearly identified and quantitatively characterized. Data were collected at 600 MHz.

remove the contribution of the detergent to the observed buoyant molecular weights (48, 49). The equilibrium association constant was estimated by globally fitting the data to a three-step binding model using the software Heteroanalysis v. 1.1.44 (J. L. Cole and J. W. Lary, University of Connecticut).

Binding of antibodies to liposome conjugates was assayed using surface plasmon resonance. Fitting of SPR data was done using the BIAeval 4.1 software (Biacore).

NMR experiments were conducted on 600-MHz and 800-MHz Varian Inova or Varian NMR spectrometers, as well as a 950-MHz Bruker Avance spectrometer. Residual dipolar couplings were obtained in a 4.5% polyacrylamide gel radially compressed using a commercial apparatus (New Era). For micelle localization, 16-doxyl steric acid (DSA) was added to a 0.5-mM sample of gp41-M-MAT in 40 mM DPC at a final concentration of 0.5 mM DSA. NOEs were binned into short-, medium-, and long-range constraints corresponding to upper limits of 3.5, 4.5, and 5.5 Å, respectively. The structure was calculated using two different methods, Xplor-NIH (50) and DISCO (46). Additional details for both structure-determination methods can be found in *SI Materials and Methods*. NMR data have been deposited in the Biological Magnetic Resonance Data Bank (BMRB) under accession number 18237. The structures have been deposited in the Protein Data Bank under two accession numbers: 2LP7 for the Xplor-NIH–based ensemble, and 2M7W for the DISCO-based ensemble.

ACKNOWLEDGMENTS. NMR experiments were conducted at the Duke NMR center and the David H. Murdoch Research Institute. We are grateful to Dr. Ron Venters for assistance with NMR data collection and interpretation. We thank Dr. Steven Harrison for comments during the preparation of this manuscript. We also thank Dr. Pei Zhou for helpful discussions about RDC analysis, Kara Anasti for assistance in performing the SPR experiments, Dr. Hua-Xin Liao for helpful discussions, and Dr. Mark Conners for providing 10E8 Mab. We gratefully acknowledge Dr. Marian Miller for original artistic contributions. This work was funded by a Collaboration for AIDS Vaccine Discovery grant from the Bill and Melinda Gates Foundation (to B.F.H. and L.D.S.) and by National Institutes of Health Grants GM-78031 and GM-65982 (to B.R.D.).

1. Freed EO (2001) HIV-1 replication. *Somat Cell Mol Genet* 26(1-6):13–33.
2. Burton DR, et al. (2004) HIV vaccine design and the neutralizing antibody problem. *Nat Immunol* 5(3):233–236.
3. Gallo SA, et al. (2003) The HIV Env-mediated fusion reaction. *Biochim Biophys Acta* 1614(1):36–50.
4. Harrison SC (2008) Viral membrane fusion. *Nat Struct Mol Biol* 15(7):690–698.
5. Zhu P, et al. (2006) Distribution and three-dimensional structure of AIDS virus envelope spikes. *Nature* 441(7095):847–852.
6. Zanetti G, Briggs JA, Grünewald K, Sattentau QJ, Fuller SD (2006) Cryo-electron tomographic structure of an immunodeficiency virus envelope complex in situ. *PLoS Pathog* 2(8):e83.
7. White TA, et al. (2010) Molecular architectures of trimeric SIV and HIV-1 envelope glycoproteins on intact viruses: Strain-dependent variation in quaternary structure. *PLoS Pathog* 6(12):e1001249.
8. Wu SR, et al. (2010) Single-particle cryoelectron microscopy analysis reveals the HIV-1 spike as a tripod structure. *Proc Natl Acad Sci USA* 107(44):18844–18849.
9. Bartesaghi A, Merk A, Borgnia MJ, Milne JLS, Subramaniam S (2013) Prefusion structure of trimeric HIV-1 envelope glycoprotein determined by cryo-electron microscopy. *Nat Struct Mol Biol* 20:1352–1357.
10. Mao Y, et al. (2012) Subunit organization of the membrane-bound HIV-1 envelope glycoprotein trimer. *Nat Struct Mol Biol* 19(9):893–899.
11. Ashkenazi A, Shai Y (2011) Insights into the mechanism of HIV-1 envelope induced membrane fusion as revealed by its inhibitory peptides. *Eur Biophys J* 40(4):349–357.
12. Frey G, et al. (2008) A fusion-intermediate state of HIV-1 gp41 targeted by broadly neutralizing antibodies. *Proc Natl Acad Sci USA* 105(10):3739–3744.
13. Buzon V, et al. (2010) Crystal structure of HIV-1 gp41 including both fusion peptide and membrane proximal external regions. *PLoS Pathog* 6(5):e1000880.
14. Muñoz-Barroso I, Salzwedel K, Hunter E, Blumenthal R (1999) Role of the membrane-proximal domain in the initial stages of human immunodeficiency virus type 1 envelope glycoprotein-mediated membrane fusion. *J Virol* 73(7):6089–6092.
15. Salzwedel K, West JT, Hunter E (1999) A conserved tryptophan-rich motif in the membrane-proximal region of the human immunodeficiency virus type 1 gp41 ectodomain is important for Env-mediated fusion and virus infectivity. *J Virol* 73(3):2469–2480.
16. Muster T, et al. (1993) A conserved neutralizing epitope on gp41 of human immunodeficiency virus type 1. *J Virol* 67(11):6642–6647.
17. Stiegler G, et al. (2001) A potent cross-clade neutralizing human monoclonal antibody against a novel epitope on gp41 of human immunodeficiency virus type 1. *AIDS Res Hum Retroviruses* 17(18):1757–1765.
18. Huang J, et al. (2012) Broad and potent neutralization of HIV-1 by a gp41-specific human antibody. *Nature* 491(7424):406–412.
19. Alam SM, et al. (2008) Human immunodeficiency virus type 1 gp41 antibodies that mask membrane proximal region epitopes: Antibody binding kinetics, induction, and potential for regulation in acute infection. *J Virol* 82(1):115–125.
20. Hinz A, et al. (2009) Characterization of a trimeric MPER containing HIV-1 gp41 antigen. *Virology* 390(2):221–227.
21. Lenz O, et al. (2005) Trimeric membrane-anchored gp41 inhibits HIV membrane fusion. *J Biol Chem* 280(6):4095–4101.
22. Guenaga J, et al. (2011) Heterologous epitope-scaffold prime:boosting immuno-focuses B cell responses to the HIV-1 gp41 2F5 neutralization determinant. *PLoS ONE* 6(1):e16074.
23. Ofek G, et al. (2010) Elicitation of structure-specific antibodies by epitope scaffolds. *Proc Natl Acad Sci USA* 107(42):17880–17887.
24. Burton DR (2010) Scaffolding to build a rational vaccine design strategy. *Proc Natl Acad Sci USA* 107(42):17859–17860.
25. Verkoczy L, et al. (2010) Autoreactivity in an HIV-1 broadly reactive neutralizing antibody variable region heavy chain induces immunologic tolerance. *Proc Natl Acad Sci USA* 107(1):181–186.
26. Verkoczy L, et al. (2013) Induction of HIV-1 broad neutralizing antibodies in 2F5 knock-in mice: Selection against membrane proximal external region-associated autoreactivity limits T-dependent responses. *J Immunol* 191(5):2538–2550.
27. Chen Y, et al. (2013) Common tolerance mechanisms, but distinct cross-reactivities associated with gp41 and lipids, limit production of HIV-1 broad neutralizing antibodies 2F5 and 4E10. *J Immunol* 191(3):1260–1275.
28. Doyle-Cooper C, et al. (2013) Immune tolerance negatively regulates B cells in knock-in mice expressing broadly neutralizing HIV antibody 4E10. *J Immunol* 191(6): 3186–3191.
29. Haynes BF, et al. (2005) Cardiolipin polyspecific autoreactivity in two broadly neutralizing HIV-1 antibodies. *Science* 308(5730):1906–1908.
30. Yang G, et al. (2013) Identification of autoantigens recognized by the 2F5 and 4E10 broadly neutralizing HIV-1 antibodies. *J Exp Med* 210(2):241–256.
31. Ofek G, et al. (2004) Structure and mechanistic analysis of the anti-human immunodeficiency virus type 1 antibody 2F5 in complex with its gp41 epitope. *J Virol* 78(19): 10724–10737.
32. Cardoso RM, et al. (2005) Broadly neutralizing anti-HIV antibody 4E10 recognizes a helical conformation of a highly conserved fusion-associated motif in gp41. *Immunity* 22(2):163–173.
33. Phogat S, et al. (2008) Analysis of the human immunodeficiency virus type 1 gp41 membrane proximal external region arrayed on hepatitis B surface antigen particles. *Virology* 373(1):72–84.
34. Alam SM, et al. (2009) Role of HIV membrane in neutralization by two broadly neutralizing antibodies. *Proc Natl Acad Sci USA* 106(48):20234–20239.
35. Ofek G, et al. (2010) Relationship between antibody 2F5 neutralization of HIV-1 and hydrophobicity of its heavy chain third complementarity-determining region. *J Virol* 84(6):2955–2962.
36. Scherer EM, Leaman DP, Zwick MB, McMichael AJ, Burton DR (2010) Aromatic residues at the edge of the antibody combining site facilitate viral glycoprotein recognition through membrane interactions. *Proc Natl Acad Sci USA* 107(4):1529–1534.
37. Güthe S, et al. (2004) Very fast folding and association of a trimerization domain from bacteriophage T4 fibritin. *J Mol Biol* 337(4):905–915.
38. Liu J, Deng Y, Dey AK, Moore JP, Lu M (2009) Structure of the HIV-1 gp41 membrane-proximal ectodomain region in a putative prefusion conformation. *Biochemistry* 48(13):2915–2923.
39. Sun ZY, et al. (2008) HIV-1 broadly neutralizing antibody extracts its epitope from a kinked gp41 ectodomain region on the viral membrane. *Immunity* 28(1):52–63.
40. Zwick MB, et al. (2001) Broadly neutralizing antibodies targeted to the membrane-proximal external region of human immunodeficiency virus type 1 glycoprotein gp41. *J Virol* 75(22):10892–10905.
41. Damberg P, Jarvet J, Gräslund A (2001) Micellar systems as solvents in peptide and protein structure determination. *Methods Enzymol* 339:271–285.
42. Beel AJ, et al. (2008) Structural studies of the transmembrane C-terminal domain of the amyloid precursor protein (APP): Does APP function as a cholesterol sensor? *Biochemistry* 47(36):9428–9446.
43. Zamoon J, Mascioni A, Thomas DD, Veglia G (2003) NMR solution structure and topological orientation of monomeric phospholamban in dodecylphosphocholine micelles. *Biophys J* 85(4):2589–2598.
44. Schibli DJ, Montelaro RC, Vogel HJ (2001) The membrane-proximal tryptophan-rich region of the HIV glycoprotein, gp41, forms a well-defined helix in dodecylphosphocholine micelles. *Biochemistry* 40(32):9570–9578.
45. Coutant J, et al. (2008) Both lipid environment and pH are critical for determining physiological solution structure of 3-D-conserved epitopes of the HIV-1 gp41-MPER peptide P1. *FASEB J* 22(12):4338–4351.
46. Martin JW, Yan AK, Bailey-Kellogg C, Zhou P, Donald BR (2011) A graphical method for analyzing distance restraints using residual dipolar couplings for structure determination of symmetric protein homo-oligomers. *Protein Sci* 20(6):970–985.
47. Dennison SM, et al. (2009) Stable docking of neutralizing human immunodeficiency virus type 1 gp41 membrane-proximal external region monoclonal antibodies 2F5 and 4E10 is dependent on the membrane immersion depth of their epitope regions. *J Virol* 83(19):10211–10223.
48. Reynolds JA, Tanford C (1976) Determination of molecular weight of the protein moiety in protein-detergent complexes without direct knowledge of detergent binding. *Proc Natl Acad Sci USA* 73(12):4467–4470.
49. Tanford C, Reynolds JA (1976) Characterization of membrane proteins in detergent solutions. *Biochim Biophys Acta* 457(2):133–170.
50. Schwieters CD, Kuszewski JJ, Clore GM (2006) Using Xplor-NIH for NMR molecular structure determination. *Prog Nucl Magn Reson Spectrosc* 48(1):47–62.